Supplementary material for: Nose T., Rabault J., Waseda T., Kodaira T., Fujiwara Y., Katsuno T., Kanna N., Tateyama K., Voermans J. & Aleekseva T. 2023. A comparison of an operational wave–ice model product and drifting wave buoy observation in the central Arctic Ocean: investigating the effect of sea-ice forcing in thin ice cover. *Polar Research 42*. Correspondence: Takehiko Nose, Department of Ocean Technology, Policy and Environment, Graduate School of Frontier Sciences, University of Tokyo, Kashiwa Chiba, 5–1–5 Kashiwanoha, Kashiwa, Chiba, Japan. E-mail tak.nose@edu.k.u-tokyo.ac.jp.

Abbreviations

AARI: Arctic and Antarctic Research Institute

ARC MFC: Arctic Ocean Wave Analysis and Forecast (produced by the Copernicus Marine Arctic Monitoring and Forecast Center)

ECMWF HRES: High Resolution Forecast (produced by the European Centre for Medium-range Weather Forecasts)

NABOS: Nansen and Amundsen Basins Observational System (part of the Arctic Observing Network)

Ice type near the ice edge

AARI ice charts during the 2021 NABOS expedition were available at http://wdc.aari.ru/datasets/d0040/arctic/png/2021/. The regional ice charts are updated monthly and made available at https://aari.ru/data/realtime (although only in Russian). The pan-Arctic and regional ice charts were obtained to estimate the ice type near the buoys during the 29 September event (Supplementary Fig. S1). The buoys were located around 82° N, 122° E during the event, and it appears that the ice type near the ice edge was young ice. The pan-Arctic ice chart was obtained from http://wdc.aari.ru/datasets/d0040/arctic/png/2021/blended_arcice_20210930-20211005_sd_90E.png and the regional ice chart from http://old.aari.ru/odata/_d0004.php?mod=0&m=Lap (by selecting year 2021 and month/day 2021.10.05 in the boxes on the right-hand side).

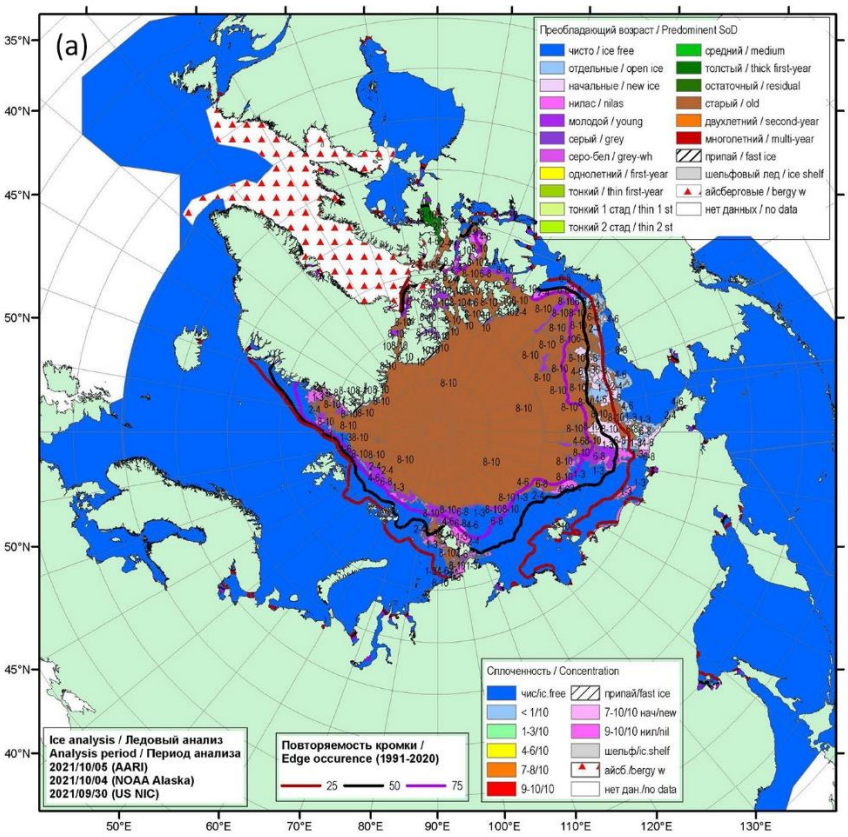

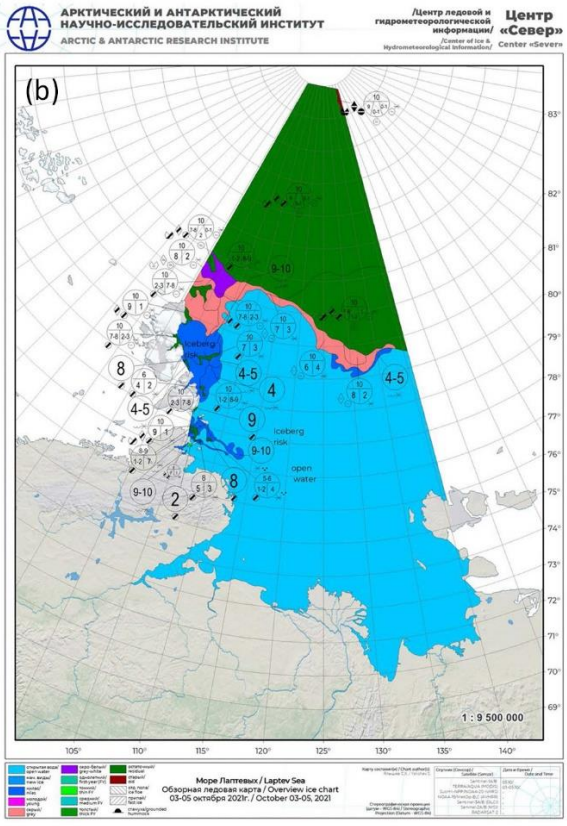

Supplementary Fig. S1. AARI ice charts for the stage of development for (a) the pan-Arctic and (b) regional waters around the 29 September event. The buoys were located around 82°N,122°E during the 29 September event, when the ice type near the ice edge was young ice.

Time series comparison of observed and modelled waves

Significant wave height H_{m0} and wave periods T_p and T_{0m1}time series (Supplementary Figs. S2, S3) were extracted from the ARC MFC wave–ice model and the ECMWF HRES wave forecast at the Zeni-v2021 and SPOT-1386 positions during their co-located deployment between 15 and 29 September 2021. The ECMWF HRES wave forecast adopts ice masks, which treat grid cells with SIC > 0.30 as land. The five H_{m0} peaks captured (Supplementary Fig. S2) show that the models were not able to reproduce reasonable values at both buoys simultaneously, and they could reproduce H_{m0} to a varying degree of accuracy only at one of the buoys.

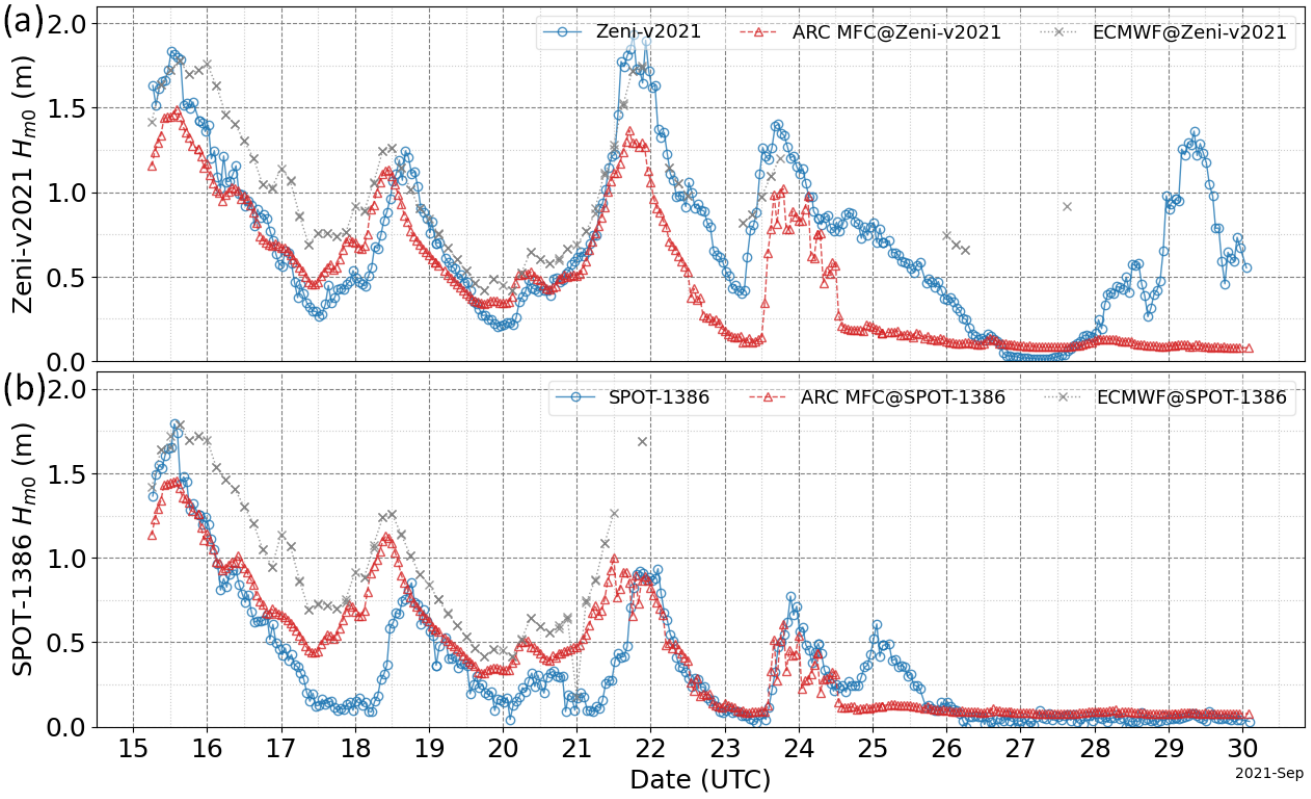

Supplementary Fig. S2. Significant wave height H_{m0} time series comparing the (a) Zeni-v2021 and (b) SPOT-1386 buoy observation (blue) and the ARC MFC (red) and ECMWF HRES wave forecast (grey) models during the co-located measurements between 15 and 29 September 2021. The missing values in the ECMWF HRES wave forecast are due to ice masks (grid cells with SIC > 0.30).

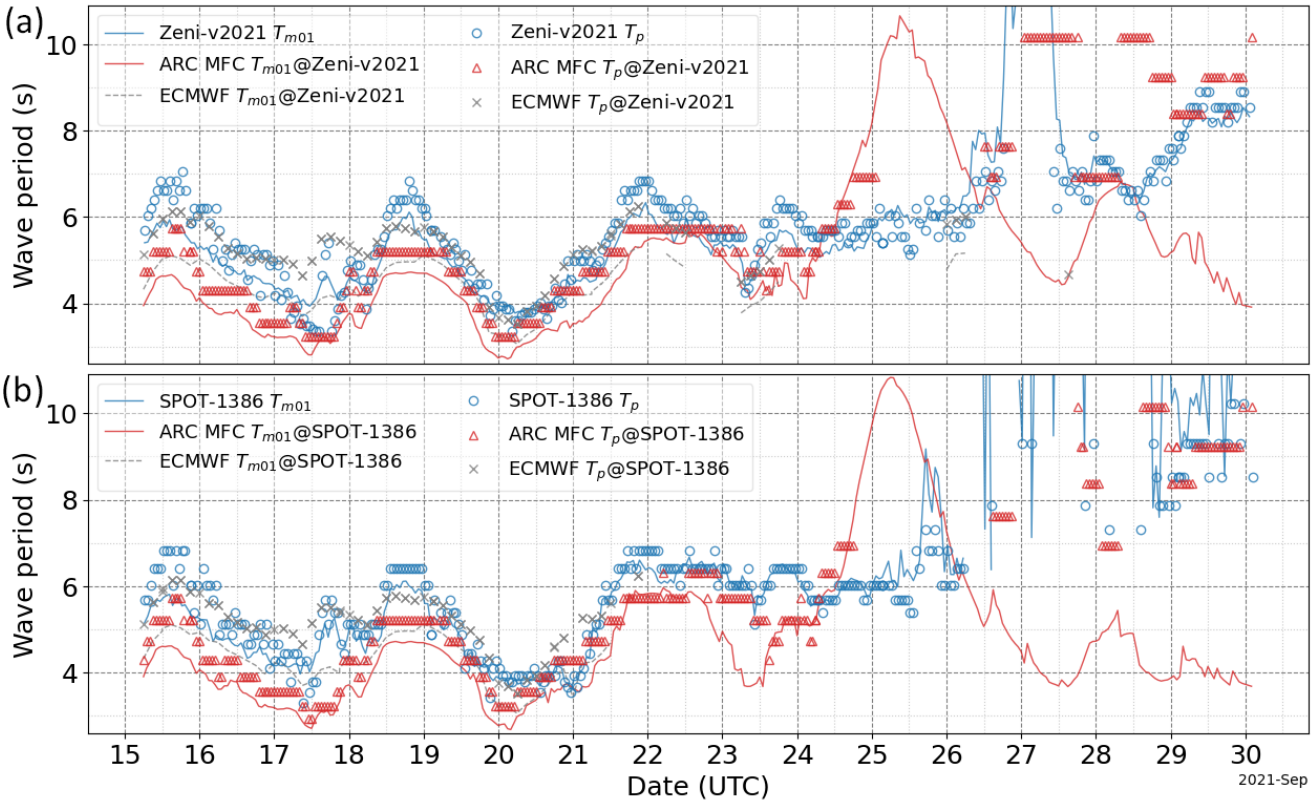

Supplementary Fig. S2. Wave periods comparing the (a) Zeni-v2021 and (b) SPOT-1386 buoy observation (blue) and the ARC MFC (red) and ECMWF HRES wave forecast (grey) models during the co-located measurements between 15 and 29 September 2021. T_p is shown as markers and T_{0m1} shown as lines. The missing values in the ECMWF HRES wave forecast are due to ice masks (grid cells with SIC > 0.30).

Lateral boundary effects of sea ice

The wind and sea-ice fields for the 15–19 September event are shown in Supplementary Fig. S4. The fetch orientation changed from along the ice edge (Supplementary Fig. S4a, c) to off-ice (Supplementary Fig. S4b, d). The ARC MFC representation of the sea-ice field has a protruding ice edge that sheltered the wave buoys from wave evolution along the ice edge immediately after the buoy deployments. In contrast, the ECWMF HRES ice edge representation is smooth, and the wave evolution towards the buoy does not appear to be sheltered by any ice-edge feature.

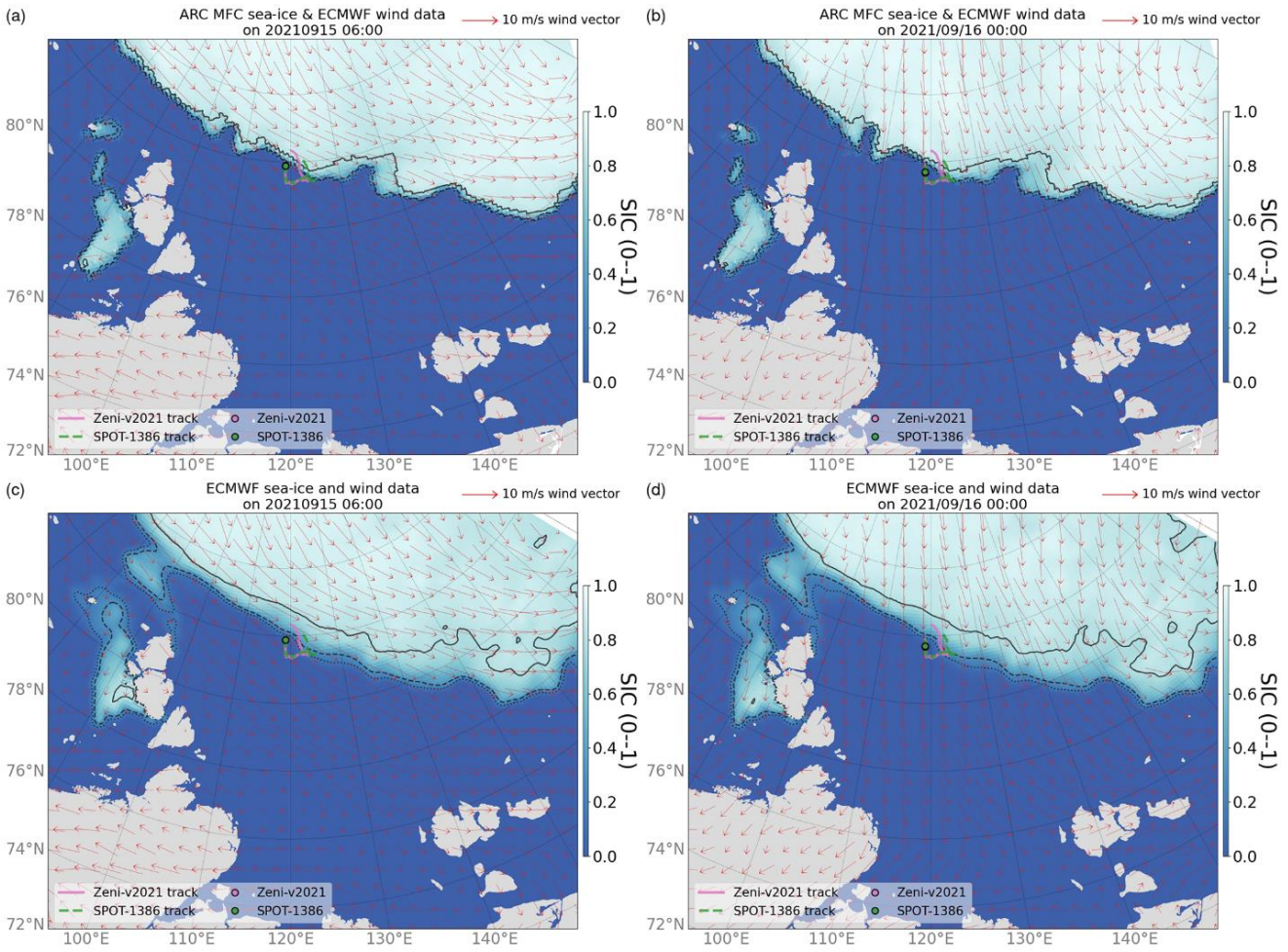

Supplementary Fig. S4. (a, b) ARC MFC and (c, d) ECMWF HRES sea-ice and wind data illustrations showing how the fetch orientation of the Zeni-v2021 and SPOT-1386 trajectories changed from (a, c) along the ice edge immediately after the deployment at 06:00 on 15 September 2021 to (b, d) off-ice by 00:00 on 16 September. Colours indicate the H_{m0} while the red vectors correspond to the ECMWF HRES wind field. The SIC contour lines are 0.15 (dotted), 0.30 (dashed) and 0.80 (solid).

Lateral boundary conditions sheltered wave evolution at the Zeni-v2021 possibly because of the misrepresentation of an ice tongue

On 21 September, west to south-west winds generated on-ice waves, i.e., waves propagating towards the ice edge, that peaked with a H_{m0} value of almost 2 m at Zeni-v2021. At this time, SPOT-1386 was located closer to the ice edge than Zeni-v2021, and its H_{m0} only peaked at ca. 1 m.

It can be seen in Supplementary Fig. S2 that Zeni-v2021 H_{m0} agrees reasonably with the ECMWF HRES wave forecast whereas the ARC MFC wave–ice model somehow underestimates the H_{m0}. A snapshot of wind, ice and wave conditions for the ECMWF HRES and ARC MFC models are provided in Supplementary Fig. S5. In the ARC MFC wave field, the Zeni-v2021 position is seaward

of the 0.10 SIC contour, so the underestimation is not caused by anomalous attenuation due to ice. Rather, the ECMWF HRES and ARC MFC SIC fields (Supplementary Fig. S5a, b) depict the ice tongue at inconsistent locations. The ARC MFC SIC field shows that the ice tongue was located near 110°E. On the basis of the wind and SIC fields, it can be conjectured that the different representation of the ice tongue affected the open water fetch; in this particular case, the ARC MFC ice tongue location was likely inaccurate considering the ECMWF HRES H_{m0} agreement with that of Zeni-v2021.

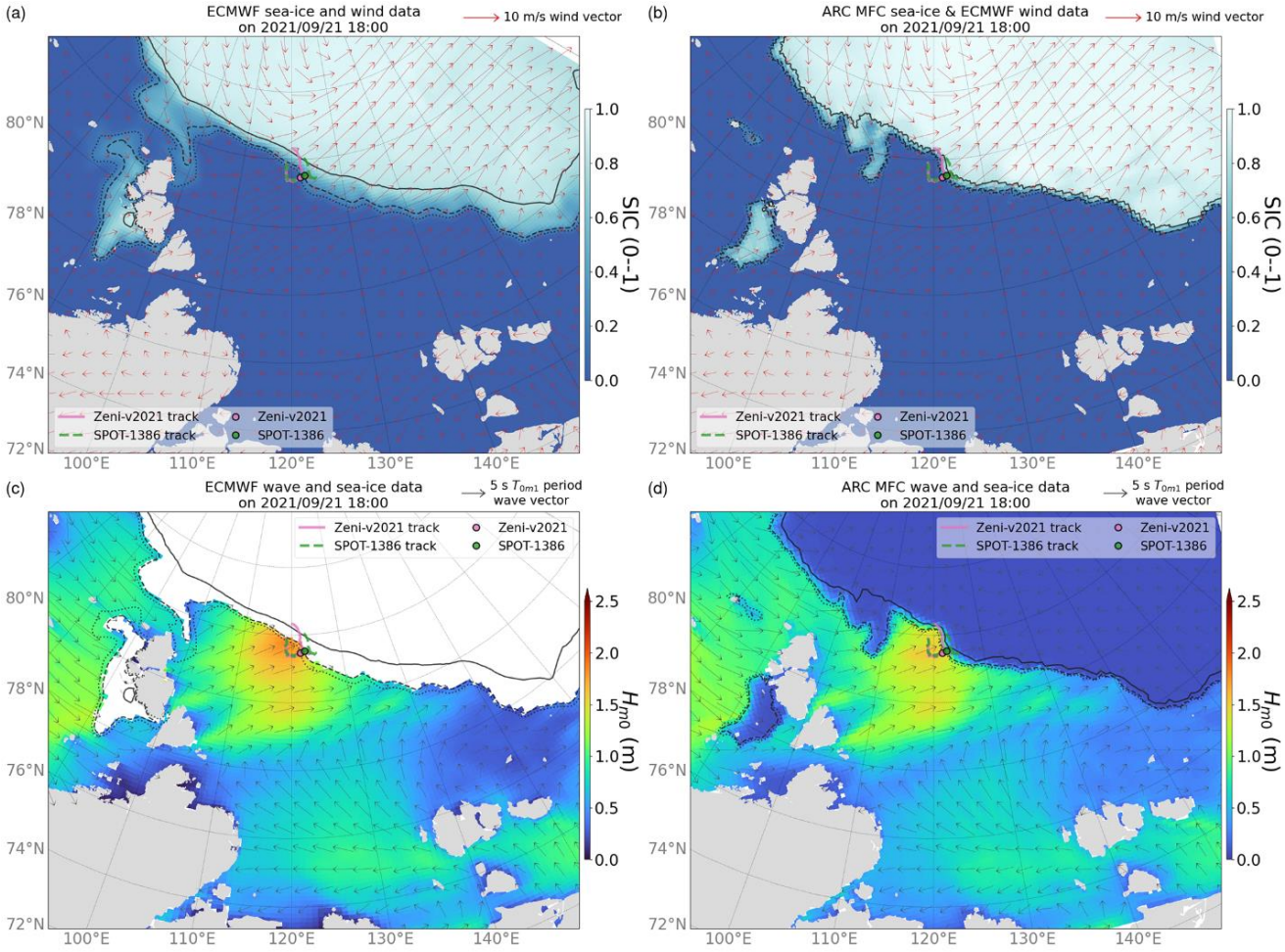

Supplementary Fig. S5. The (a, c) ECMWF HRES and (b, d) ARC MFC representations of the ice tongue on 18:00 on 21 September 2021: (a) and (b) the wind (red vectors; from the ECMWF HRES atmospheric forecast) and ice (colours) conditions and (c) and (d) the waves, with the colours correspond to H_{m0} while the grey vectors indicate the mean wave directions, for which vector lengths are scaled by the corresponding T_{0m1}. The SIC contour lines are 0.15 (dotted), 0.30 (dashed) and 0.80 (solid).

Disparate SIT distributions between ARC MFC and neXtSIM sea-ice fields

A comparison of ARC MFC and neXtSIM sea-ice fields during the 29 September at the regional scale is presented in Fig. S6 to support the section about the disparate scale between wave dissipation parameterization and the SIT forcing in the main article. It is apparent that ARC MFC SIT resolution below 0.5 m is considerably poorer than that of neXtSIM. It is conjectured in the main text that this may be due to the following. neXtSIM consists of a newly formed ice category in which the ice formation is calculated from the atmosphere and ocean forcing, whereas the ARC MFC model uses a one-thickness category model in which the minimum thickness of newly formed ice is set as 0.5 m (Drange & Simonsen 1996; Sakov et al. 2012). We also discuss another possible contributing factor, which is the data assimilation method. The poor thin ice distribution may be caused by the data assimilation method assuming a correlation between observed SIC and unobserved SIT in the ARC MFC ocean analysis.

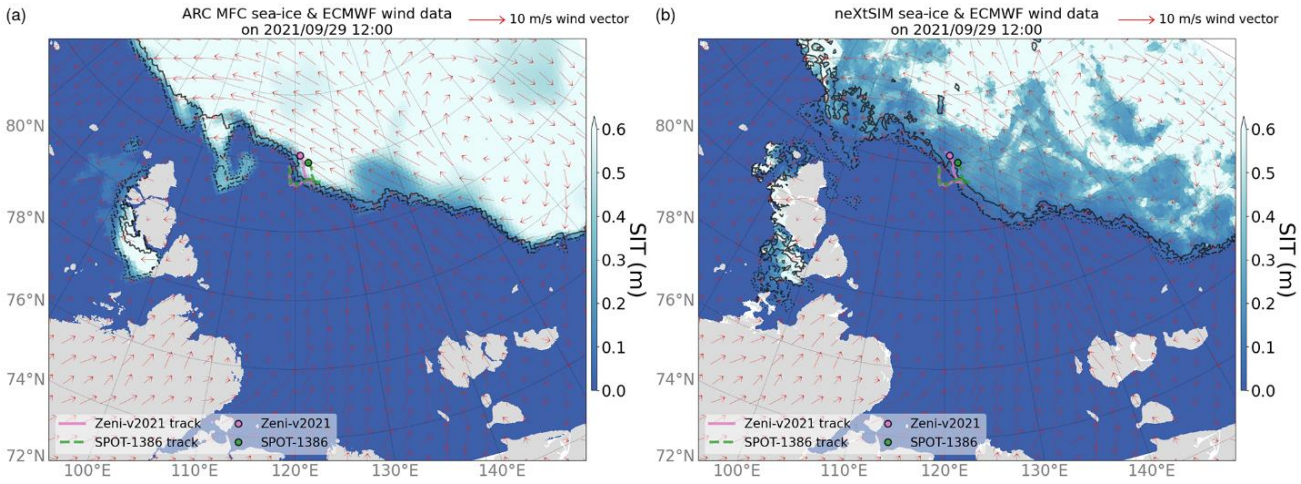

Supplementary Fig. S6. A regional-scale comparison of SIT (colours) fields for the (a) ARC MFC wave–ice model sea-ice forcing and (b) the neXtSIM sea-ice model. There is a marked difference in the thin ice distributions given by the two models. The red vectors are the ECMWF HRES model wind data. The SIC contour lines are 0.15 (dotted), 0.30 (dashed) and 0.80 (solid).